Inorganic Chemistry

Article

pubs.acs.org/IC

Spectroscopic Characterization of a Monomeric, Cyclopentadienyl-Based Rhenium(V) Dioxo Complex

Suresh Raju,[†] Johann T. B. H. Jastrzebski,[†] Martin Lutz,[‡] Léon Witteman,[†] Johannes R. Dethlefsen,[§] Peter Fristrup,[§] Marc-Etienne Moret,*[,†] and Robertus J. M. Klein Gebbink*[,†]

[†]Organic Chemistry and Catalysis, Debye Institute for Nanomaterials Science, Faculty of Science, Utrecht University, Universiteitsweg 99, Utrecht 3584 CG, The Netherlands

[‡]Crystal and Structural Chemistry, Bijvoet Center for Biomolecular Research, Utrecht University, Padualaan 8, Utrecht 3584 CH, The Netherlands

[§]Department of Chemistry, Technical University of Denmark, Kemitorvet 207, DK-2800 Kgs. Lyngby, Denmark

S *Supporting Information*

ABSTRACT: Mononuclear, coordinatively unsaturated rhenium(V) dioxo species of the type $XReO_2$ (X = Me, substituted cyclopentadienyl) have long been postulated as intermediates in rhenium-catalyzed deoxydehydration, but their characterization was precluded because of aggregation into dimeric or oligomeric structures. Using the bulky 1,2,4-tri-*tert*-butylcyclopentadienyl (Cp^{ttt}) ligand, the rhenium(V) dioxo species $(Cp^{ttt})ReO_2$ could now be observed, in equilibrium with the dimeric form $[(Cp^{ttt})Re(O)\mu\text{-}O]_2$, and characterized by NMR, IR, and UV−vis spectroscopies, as well as electrospray ionization mass spectrometry. $(Cp^{ttt})ReO_2$ is shown to be the primary product of reduction of the rhenium(VII) complex $(Cp^{ttt})ReO_3$ with PPh_3 and demonstrated to react with ethylene glycol significantly faster than its dimeric counterpart, supporting its role as an intermediate in rhenium-catalyzed deoxydehydration reactions.

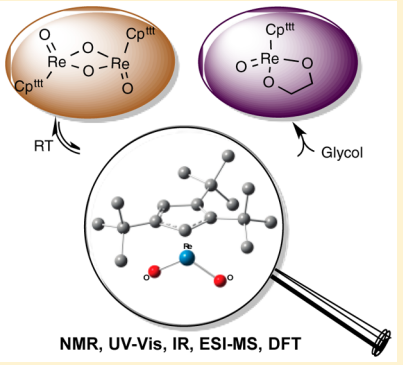

INTRODUCTION

Cellulosic biomass is emerging as a potential renewable feedstock for the chemical industry.[1a] In this context, the search for an efficient route from polyhydroxyl sugars and their derivatives to the corresponding polyolefins motivates a renewed attention to reductive deoxygenation reactions.[1b,c] Among these, deoxydehydration (DODH) of diols to olefins catalyzed by organometallic oxorhenium complexes appears as one of the most promising approaches.[1c−e] The first catalytic DODH was developed in 1996 by Andrews et al. by using $(Cp^*)ReO_3$ (Cp* = 1,2,3,4,5-pentamethylcyclopentadienyl) as a precatalyst for reduction of a vicinal diol to the corresponding olefin with the use of PPh_3 as a sacrificial reductant.[2a] The low catalytic turnover numbers (TON ∼ 55) were assigned to fast catalyst decomposition through the formation of insoluble tri- and tetranuclear oxorhenium clusters.[2b,c] More recent work has focused mainly on methyltrioxorhenium (MTO), demonstrating its activity in DODH reactions with various reductants.[3] Aiming at the development of more readily tunable catalysts, we recently revisited the use of trioxorhenium complexes with substituted Cp ligands and identified $(Cp^{ttt})ReO_3$ (**1**; Cp^{ttt} = 1,2,4-tri-*tert*-butylcyclopentadienyl) as an improved DODH catalyst (for 1,2-octanediol conversion to octenes, TONs up to 1400 per rhenium can be reached).[4]

Central to the further development of DODH catalysts is a good understanding of the reaction mechanism(s) by which the catalysts operate. On the basis of stoichiometric work by Herrmann and co-workers[5a,b] and Gable and co-workers,[5c,d] a DODH cycle is generally thought to consist of three steps: (a) reduction of the rhenium(VII) trioxo species to a rhenium(V) dioxo species, (b) condensation with the diol to form a rhenium(V) diolate, and (c) extrusion of the olefin product to regenerate a rhenium(VII) trioxo species (Scheme 1).[2a,3d,6]

Scheme 1. Proposed Rhenium-Catalyzed DODH Mechanism

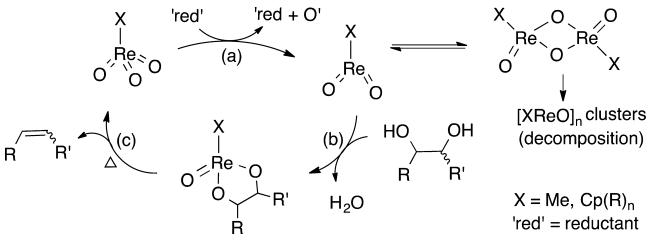

Alternatively, Abu-Omar and co-workers proposed the olefin extrusion step to occur via a putative rhenium(III) diolate species for MTO-catalyzed DODH.[6] Observation and characterization of the key rhenium(V) dioxo intermediates would be highly desirable to consolidate our mechanistic understanding but is hampered by their tendency to aggregate in di- or

Received: October 13, 2015
Published: October 30, 2015

DOI: 10.1021/acs.inorgchem.5b02366
Inorg. Chem. 2015, 54, 11031−11036

Scheme 2. Synthesis of Reduced Rhenium(V) Oxo Complexes Bearing the Cp^{ttt} Ligand

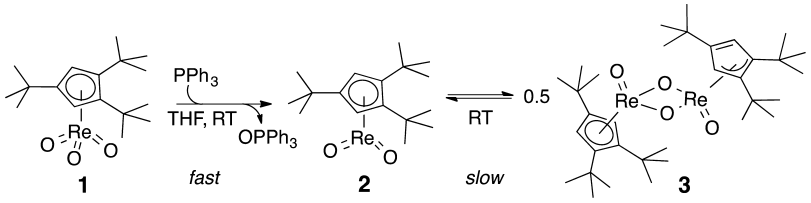

multinuclear species, which is also considered as the main route toward catalyst decomposition.[2b,7] For example, even though adduct formation reactions with nucleophilic reagents (e.g., phosphines[6] and alkynes[3d,8]) allowed the observation of monomeric rhenium(V) dioxo species derived from MTO, characterization of coordinatively unsaturated $MeReO_2$ remains elusive.[9] In contrast, the reduction of $(Cp^*)ReO_3$ with PPh_3 results in the well-characterized dimer $[(Cp^*)Re(O)\mu\text{-}O]_2$ without any other additional coordinating ligand.[5a,10a,b] Interestingly, Gable et al. observed that heating an NMR sample of $[(Cp^*)Re(O)\mu\text{-}O]_2$ caused the appearance of small amounts of a new species that was tentatively assigned as $(Cp^*)ReO_2$ but could not be further characterized.[11] We now report that using the bulkier Cp^{ttt} ligand allows the direct observation and spectroscopic characterization of the monomeric $(Cp^{ttt})ReO_2$ (**2**) species, which is demonstrated to engage in the diol condensation (step b) faster than its dimeric counterpart $[(Cp^{ttt})Re(O)\mu\text{-}O]_2$ (**3**), supporting its involvement as a key intermediate in DODH reactions.

RESULTS AND DISCUSSION

First, the procedure of Herrmann et al. for the synthesis of $[(Cp^*)Re(O)\mu\text{-}O]_2$[2c] was slightly modified to synthesize **3** as a dark-brown solid (67% yield): equivalent amounts of PPh_3 and **1** were reacted in tetrahydrofuran (THF) for 16 h (Scheme 2). Recrystallization in hexane/acetone (2:1) at −30 °C afforded crystals of sufficient quality for X-ray diffraction. The solid-state structure of **3** displays a Re_2O_4 unit sandwiched between two Cp^{ttt} ligands (Figure 1). The ring-slippage parameter Δ[12a,b] of

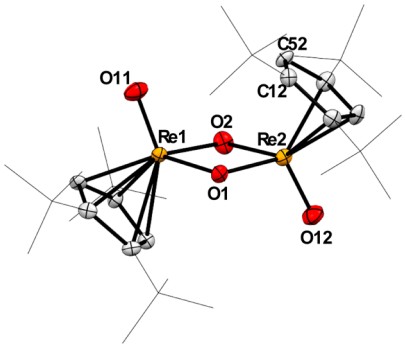

Figure 1. ORTEP picture of **3**, drawn at the 50% probability level. Hydrogen atoms are omitted, and the *t*Bu groups are shown as wire frame for clarity.

the Cp ring bound to Re1 is 0.25 Å, which is generally described as a slipped η^5- or η^2-olefin/η^3-allyl bonding,[5a] whereas the Cp ring bound to Re2 is strongly slipped with Δ = 0.45 Å, indicating η^3 bonding. The long Re2−C12 [2.587(7) Å] and Re2−C52 [2.468(7) Å] distances, and the short C12−C52 bond [1.408(9) Å] approaching double-bond behavior, support the description of this Cp ring as η^3-bonded.[13] Such Cp ring slippage is common in oxorhenium complexes because of the trans influence of π-donating oxo ligands.[5a] Consideration of a space-filling model of **3** suggests that steric repulsion between *t*Bu groups of different Cp^{ttt} ligands is responsible for the observed η^3 bonding, with a rather short C92···C111 distance of 3.725 Å between methyl groups of the two Cp^{ttt} ligands (Figure S1).

The unsymmetrical bonding modes of the two Cp ligands contrasts with the η^5/η^5 bonding observed in the analogous complex $[(Cp^*)Re(O)\mu\text{-}O]_2$. The Re1−Re2 distance [3.1086(4) Å] in **3** is somewhat shorter than that in $[(Cp^*)Re(O)\mu\text{-}O]_2$ (3.142 Å), which had been proposed to involve some degree of metal−metal bonding.[11,14] To clarify this issue, a natural bonding orbital (NBO)[15a] analysis was performed on the electron density obtained for **3** at the B3LYP/6-31G(d,p);SDD(Re) level.[15b] It identified one filled lone-pair NBO of d character on each rhenium atom, as expected for two rhenium(V) centers (Figure S1). Second-order perturbation analysis found donation from the rhenium-based lone pair to Cp-based orbitals (back-donation) but found no significant (<5 kcal/mol) donor−acceptor interaction between the filled d orbital of one rhenium atom and empty d or σ^*(Re−O) orbitals of the other, indicating the absence of significant Re−Re bonding.

In agreement with the X-ray crystal structure, the electrospray ionization mass spectrometry (ESI-MS) spectrum of **3** showed a signal at *m*/*z* 904.3503, corresponding to the expected dimeric species (M^+; calcd *m*/*z* 904.3453). IR (KBr pellet) vibrations for bridging oxygen atoms (Re−O−Re) were observed at 637, 652, and 670 cm^{-1}, and the terminal oxo vibrations appeared at 930 and 947 cm^{-1}. The doubling of the terminal Re═O band contrasts with the single band observed at 930 cm^{-1} for $[(Cp^*)Re(O)\mu\text{-}O]_2$, likely reflecting the lower symmetry of **3**.[10a]

The ^{1}H NMR spectrum of **3** in C_6D_6 at room temperature displays one signal for Cp−H at 5.32 ppm and two for the *t*Bu groups at 1.43 and 1.41 ppm, respectively, suggesting a symmetrical structure in solution at first sight. However, cooling a sample of **3** in THF-d_8 from −20 to −110 °C results in a gradual splitting of the Cp−H resonance into three signals at 5.03, 5.73, and 6.27 ppm in a 2:1:1 ratio (Figure S2). Thus, the two Cp^{ttt} ligands are not equivalent in solution, and rotation around the Re−Cp axis becomes slow at low temperature for at least one of them, supporting the idea that the unsymmetrical structure observed for **3** in the solid state also exists in solution.

When a clean solution of **3** in C_6D_6 is stored at room temperature, a new Cp−H signal gradually appears at 4.81 ppm in the ^{1}H NMR spectrum, together with corresponding *tert*-butyl signals at 1.22 and 1.19 ppm, reaching equilibrium after ca. 4 h. The new signals grow with increasing temperature, and a DOSY NMR experiment (Figure S3) associates them with a diffusion coefficient 1.6 times larger than that of **3**, which confirms their assignment to the monomeric species **2**.

DOI: 10.1021/acs.inorgchem.5b02366
Inorg. Chem. 2015, 54, 11031−11036

Equilibrating an NMR sample at 75 °C followed by rapid cooling afforded an enriched sample on which ^{1}H and ^{13}C NMR characterization data for **2** were recorded (see the Supporting Information, SI). Van't Hoff analysis of the equilibrium between **3** and **2** yields a reaction enthalpy of $\Delta_r H = 11.6 \pm 0.2$ kcal/mol and a positive entropy of reaction of $\Delta_r S = 27.7 \pm 0.6$ cal/(mol K) consistent with a dissociation reaction (Figure 2 and Table S1). The obtained enthalpy of

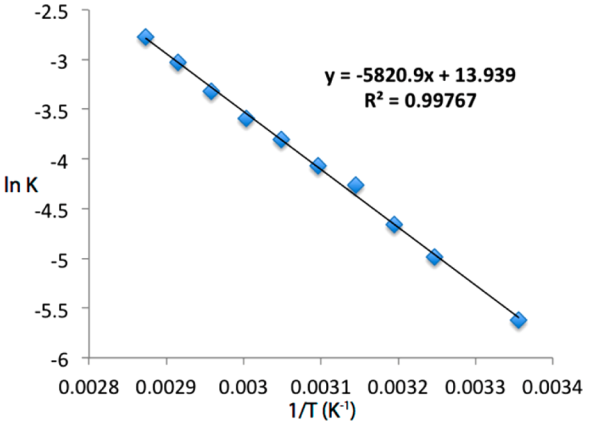

Figure 2. Van't Hoff plot for the equilibrium between **3** and **2** in C_6D_6 (total rhenium concentration: 7 mM). The concentrations of **3** (5.32 ppm) and **2** (4.81 ppm) were measured from the NMR integrals against the internal standard (mesitylene).

reaction is significantly lower than for the corresponding Cp* ligated complexes ($\Delta_r H = 16.8 \pm 0.3$ kcal/mol),[11] supporting the notion that the increased steric bulk of the Cp^{ttt} ligand favors formation of the monomer. Density functional theory (DFT) calculations at the B3LYP/6-31G(d,p);SDD(Re) level correctly predict the trend in $\Delta_r H$ (Cp^{ttt}, 14.8 kcal/mol; Cp*, 19.7 kcal/mol).

Attempts to isolate **2** by extraction and/or crystallization from mixtures of **2** and **3** or by rapid reduction of **1** with PPh_3 or an insoluble PPh_3 resin were unsuccessful (see the SI, p S6). Also, the addition of PPh_3 to the equilibrium mixture in C_6D_6 (7 mM; 2 equiv based on rhenium) at ambient temperature does not lead to adduct formation of either **2** or **3**, even though the corresponding in situ generated methyldioxorhenium species is known to form $MeReO_2(PR_3)_2$ (R = phenyl, cyclohexyl) complexes.[6] However, complex **2** could additionally be characterized by a range of spectroscopic techniques.[16] First, equilibration between **2** and **3** was followed by variable-temperature UV−vis spectroscopy: absorption of **3** at 431 nm decreases with increasing temperature, while a new band grows at 383 nm (Figure 3). The spectral changes are reversible and display a nearly isosbestic point at 407 nm. Then, vibrational data were obtained from enriched solid samples with **2**/**3** ratios of 2.9:1 and 7.2:1 that were prepared by rapid cooling and drying of solutions equilibrated at higher temperatures (see the SI, p S6). In addition to the known bands of **3** at 930 and 950 cm^{-1} (slightly shifted from 947 cm^{-1}), the IR spectrum (KBr pellet) of these mixtures displays two new bands at 914 and 940 cm^{-1} that are assigned to the antisymmetrical and symmetrical modes, respectively, arising from two coupled Re═O oscillators (Figure 3). This interpretation is supported by DFT calculations performed at the B3LYP/6-31G(d,p);SDD-(Re) level, which predict a splitting of 31 cm^{-1} (ν_{asym} = 946 cm^{-1}; ν_{sym} = 977 cm^{-1}) for **2**, in good agreement with the

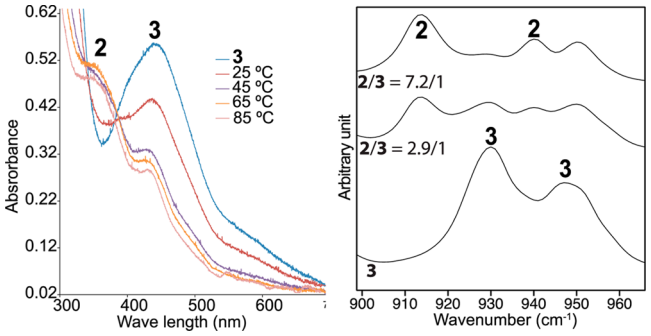

Figure 3. Left: UV−vis spectra of pure **3** (blue) and of equilibrated mixtures of **2** and **3** at variable temperature in toluene. Right: Solid-state (KBr) Fourier transform infrared spectra of pure **3** and samples enriched in **2**. The indicated **2**/**3** ratios were measured independently by solution ^{1}H NMR.

experimental value of 26 cm^{-1} (Figures S6−S8). The computed terminal Re−O (Re−O2, 1.726 Å; Re−O3, 1.734 Å) and Cp(centroid)−Re (2.046 Å) distances of **2** are comparable to those of **3** (vide supra). ESI−MS analysis of the mixture of **2** and **3** showed a signal at m/z 453.1815 corresponding to the protonated monomeric species **2** [$(M + H)^+$; calcd m/z 453.1804]. The DFT-optimized structure of complex **2** displays a two-legged piano-stool geometry with a small ring-slippage value of Δ = 0.16 Å (Figure 4).

The first-order rate constant for the dissociation of **3** into **2** was evaluated to $k = (1.31 \pm 0.05) \times 10^{-4}$ s^{-1} at room temperature from the following equation (Figures S9 and S10):[17]

$$(X_e/A_0)\ln(X_e/X_e - X) = kt \quad (1)$$

where A_0, X_e, and X are the concentration of **3** at initial, equilibrium, and time t, respectively. The corresponding free enthalpy of activation ($\Delta G^{\ddagger}$) (22.5 ± 1.9 kcal/mol) may at first sight appear surprisingly large. To gain more insight, the mechanism of dissociation of **3** was studied by DFT. A single transition state was located using the QST3 method, and an intrinsic reaction coordinate (IRC) calculation confirmed the concerted nature of this transformation. The corresponding free enthalpy of activation at room temperature ($\Delta G^{\ddagger}$ = 25.6 kcal/mol) is in good agreement with the experimental value. In the optimized transition state (Figure 4), one of the Re−O bonds of the diamond core is fully broken (Re2−O1 = 2.956 Å), while the opposite one is only slightly elongated (Re1−O2 = 1.987 Å). As a result, the Re1 and Re2 centers display three-legged and two-legged piano-stool geometries, respectively. The three terminal Re−O bonds approach double-bond character (Re1−O1, 1.783; Re1−O11, 1.746; Re2−O12, 1.712 Å), while the bridged oxygen O2 is unsymmetrically bonded between rhenium atoms (Re1−O2, 1.987; Re2−O2, 1.853 Å). The ring-slippage values (Δ = 0.22 and 0.34 Å) in the transition state are getting closer to the value in **2** (Δ = 0.16 Å). These observations support the description of the dissociation of **3** as a concerted asynchronous process.

Having established the nature of complex **2**, a series of experiments were performed to determine whether it is a plausible intermediate in DODH reactions. First, complex **2** was shown to be the initial product of the reaction of **1** with PPh_3: an NMR spectrum recorded after 5 min of mixing time in toluene-d_8 at room temperature showed complete conversion of **1** to **2** (97%). Complex **2** then slowly dimerized to **3** to reach

DOI: 10.1021/acs.inorgchem.5b02366
Inorg. Chem. 2015, 54, 11031−11036

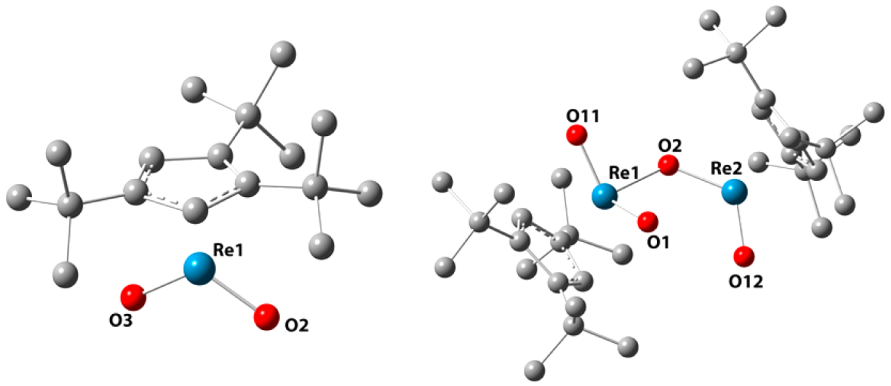

Figure 4. DFT-optimized structure of **2** (left) and transition state (right) for the dissociation of **3** into **2**.

equilibrium after 7 h (Figure S11). Moreover, the reduction of **1** by PPh_3 was also monitored in situ by IR spectroscopy at 0 °C in toluene. Clean formation of **2** corresponding to the conversion of **1** was observed within 8 min (i.e., by following the Re═O vibrations), and it exhibited almost no further dimerization of **2** for 30 min (Figures S12 and S13). The stepwise formation of **2** followed by equilibration with **3**, as shown in Scheme 2, is hence confirmed.

Second, the formation and characterization of **2** allowed us to compare its reactivity to that of its dimeric congener **3**. To an equilibrated mixture of **3** and **2** (**3**/**2** ratio: 1.3) in C_6D_6 was added excess ethylene glycol (ca. 15 equiv), and the reaction was monitored by NMR spectroscopy, showing clean formation of the corresponding rhenium(V) diolate (Cp^{ttt})ReO($C_2H_4O_2$) (**4**; Scheme 3), which was identified by comparison with an

Scheme 3. Glycol Condensation Reaction of 2 Resulting in the Rhenium(V) Diolate 4

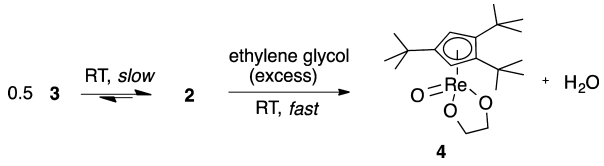

isolated and fully characterized sample (see the SI).[18a,b] The reaction of monomeric **2** with ethylene glycol is significantly faster than that of the dimer **3** and also faster than the equilibrium reaction of **3** and **2**, which is consistent with **2** being the active species in the DODH cycle while **3** acts as a reservoir (Figure 5).

Finally, thermolysis of the diolate complex **4** above 90 °C (in toluene-d_8) extrudes ethylene and cleanly regenerates the trioxo compound **1**, closing the proposed catalytic cycle. Activation parameters for this reaction were obtained from an Eyring plot derived from variable-temperature NMR (90−120 °C): $\Delta H^{\ddagger}$ = 29.1 ± 2.1 kcal/mol and $\Delta S^{\ddagger}$ = −1.71 ± 2.1 cal/(mol K) (Figure S15). These activation parameters are close to those obtained for the analogous reaction of Cp*ReO(ethanediolate) [$\Delta H^{\ddagger}$ = 28.0 ± 0.4 kcal/mol and $\Delta S^{\ddagger}$ = −2.1 ± 1.2 cal/(mol K)].[5c,d] Ethylene extrusion is generally thought to be rate-limiting in DODH reactions;[2a] the fact that it is only minimally affected by the steric difference between the Cp^{ttt} and Cp* ligands supports the idea that the increased TONs achieved with Cp^{ttt} mostly stem from an increased stability toward catalyst decomposition. It is, however, plausible that the steric

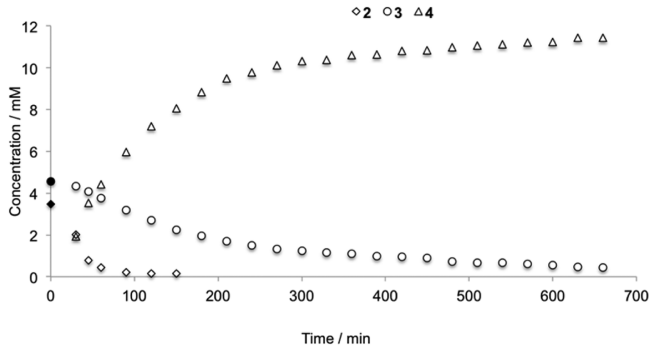

Figure 5. Concentration profile of the reaction of a mixture of **2** and **3** in C_6D_6 at 25 °C with excess ethylene glycol to form **4**. The concentrations were determined by ^1H NMR integration against an internal standard (mesitylene). Filled data points at time zero indicate equilibrium concentrations prior to the addition of ethylene glycol.

profile of the supporting ligand would more significantly impact olefin extrusion for larger polyol substrates.

CONCLUSION

In summary, the sterically demanding Cp^{ttt} ligand destabilizes the dimeric rhenium(V) dioxo complex **3** to such an extent that the corresponding monomer **2** can be observed in appreciable concentration and spectroscopically characterized. This destabilization is thought to originate from steric repulsion between the two Cp^{ttt} ligands in **3**. Monomeric species **2** was shown to be the initial reaction product of **1** with the prototypical reductant PPh_3 and to undergo condensation with ethylene glycol at a faster rate than dimer **3**, supporting its involvement in the catalytic cycle for diol DODH catalyzed by complex **1**. The obtained diolate complex **4** was shown to undergo ethylene extrusion with an activation barrier similar to that of the Cp* analogue.

Thus, the bulky Cp^{ttt} ligand is thought to improve the catalyst performance by lowering the fraction of the metal present in the inactive dimeric form under catalytic conditions. This may also slow down catalyst decomposition to oligomeric species that has been proposed to proceed via dimeric rhenium(V) species.[2b,7,8] The observation and characterization of the long-sought intermediate **2** paves the way for an in-depth mechanistic understanding of this rhenium-catalyzed DODH reaction aimed at rational catalyst optimization, which is currently under investigation in our laboratory.

DOI: 10.1021/acs.inorgchem.5b02366
Inorg. Chem. 2015, 54, 11031−11036

EXPERIMENTAL SECTION

General Considerations. All reactions were carried out either in a nitrogen-filled MBraun glovebox with <0.1 ppm concentrations of H_2O and O_2 or with Schlenk-line techniques under a nitrogen atmosphere. $Cp^{ttt}ReO_3$ was prepared based on the previously reported procedure.[4] All other chemicals and solvents including NMR solvents were degassed either by prolonged exposure to a vacuum or by freeze−pump−thaw cycles. Benzene, THF, and THF-d_8 were distilled over sodium/benzophenone. Toluene and hexane solvents were obtained from an MBraun MB SPS-800 solvent purifier and stored over 4 Å molecular sieves. NMR solvents like C_6D_6 and toluene-d_8 were degassed and stored over molecular sieves. Unless otherwise stated, all other commercial chemicals were used without further purification. NMR spectra were recorded on a Varian VNMRS400 (400 MHz). IR spectra were recorded using a PerkinElmer Spectrum One Fourier transform infrared spectrometer in the range of 450−4000 cm^{-1} (KBr). UV−vis spectra were recorded on a PerkinElmer Lambda 650 spectrometer. ESI-MS spectra were recorded using a Waters LCT Premier XE instrument.

Synthesis of 3. To a mixture of **1** (0.4 g, 0.855 mmol) and PPh_3 (0.224 g, 0.855 mmol) in a 20 mL scintillation vial was added THF (12 mL) with magnetic stirring. The color changed rapidly to yellow brown followed by dark brown in a few minutes. After the reaction was stirred for 14 h, THF was evaporated in vacuo followed by repeated extraction of the residue with cold hexane (3 × 5 mL). The combined hexane solution was dried under vacuum to obtain **3** as a dark-brown solid (0.26 g, 67%). Crystals of **3** suitable for X-ray diffraction were obtained from a 1:2 mixture of acetone and hexane at −30 °C. ^1H NMR (400 MHz), C_6D_6 (7.16 ppm): 1.41 (s, 9H, *t*Bu), 1.43 (s, 18H, *t*Bu), 5.32 (s, 2H, CpH). ^{13}C NMR (400 MHz), C_6D_6 (128.06 ppm): 30.8, 33.22, 33.97, 35.45, 100.34, 124.30, 126.66 ppm. IR (ATR/KBr): 545, 637, 652, 670, 930, 947, 1248, 1367, 1392, 1463, 1485, 2872, 2925, 2961, 3097 cm^{-1}; HR-ESI-MS. Calcd for $[C_{34}H_{58}Re_2O_4]^+$: *m*/*z* 904.3453. Found: *m*/*z* 904.3503.

ASSOCIATED CONTENT

Supporting Information

The Supporting Information is available free of charge on the ACS Publications website at DOI: 10.1021/acs.inorgchem.5b02366.

Experimental procedures for the synthesis of **2**−**4**, spectroscopic characterizations, and DFT computational details (PDF)

X-ray crystallographic data in CIF format (CIF)

AUTHOR INFORMATION

Corresponding Authors

*E-mail: m.moret@uu.nl.

*E-mail: r.j.m.kleingebbink@uu.nl.

Author Contributions

The manuscript was written through contributions of all authors. All authors have given approval to the final version of the manuscript.

Notes

The authors declare no competing financial interest.

ACKNOWLEDGMENTS

This research has been performed within the framework of the CatchBio program. We gratefully acknowledge support of the Smart Mix Program of The Netherlands Ministry of Economic Affairs and The Netherlands Ministry of Education, Culture, and Science. DFT work was carried out on the Dutch national e-infrastructure with support of the SURF Foundation. S.R. acknowledges COST action CM1205 for an STSM grant. M.-E.M. acknowledges funding from the European Union Seventh Framework Programme (FP7/2007−2013) under Grant Agreement PIIF-GA-2012-327306 (an IIF-Marie Curie grant). P.F. was supported by a Sapere Aude research leader grant from the Danish Council for Independent Research (Grant 11-105487).

REFERENCES

(1) (a) Ruppert, A. M.; Weinberg, K.; Palkovits, R. *Angew. Chem., Int. Ed.* **2012**, *51*, 2564−2601. (b) Metzger, J. O. *ChemCatChem* **2013**, *5*, 680−682. (c) Dutta, S. *ChemSusChem* **2012**, *5*, 2125−2127. (d) Raju, S.; Moret, M.-E.; Klein Gebbink, R. J. M. *ACS Catal.* **2015**, *5*, 281−300. (e) Dethlefsen, J. R.; Fristrup, P. *ChemSusChem* **2015**, *8*, 767−775. (f) Boucher-Jacobs, C.; Nicholas, K. M. *Top. Curr. Chem.* **2014**, *353*, 163−184.

(2) (a) Cook, G. K.; Andrews, M. A. *J. Am. Chem. Soc.* **1996**, *118*, 9448−9450. (b) Gable, K. P.; Zhuravlev, F. A.; Yokochi, A. F. T. *Chem. Commun.* **1998**, 799−800. (c) Herrmann, W. A.; Serrano, R.; Küsthardt, U.; Guggolz, E.; Nuber, B.; Ziegler, M. L. *J. Organomet. Chem.* **1985**, *287*, 329−344.

(3) (a) Ziegler, J. E.; Zdilla, M. J.; Evans, A. J.; Abu-Omar, M. M. *Inorg. Chem.* **2009**, *48*, 9998−10000. (b) Arceo, E.; Ellman, J. A.; Bergman, R. G. *J. Am. Chem. Soc.* **2010**, *132*, 11408−11409. (c) Yi, J.; Liu, S.; Abu-Omar, M. M. *ChemSusChem* **2012**, *5*, 1401−1404. (d) Shiramizu, M.; Toste, F. D. *Angew. Chem., Int. Ed.* **2012**, *51*, 8082−8086. (e) Shiramizu, M.; Toste, F. D. *Angew. Chem., Int. Ed.* **2013**, *52*, 12905−12909. (f) Boucher-Jacobs, C.; Nicholas, K. M. *ChemSusChem* **2013**, *6*, 597−599. (g) McClain, J. M.; Nicholas, K. M. *ACS Catal.* **2014**, *4*, 2109−2112.

(4) Raju, S.; Jastrzebski, J. T. B. H.; Lutz, M.; Klein Gebbink, R. J. M. *ChemSusChem* **2013**, *6*, 1673−1680.

(5) (a) Herrmann, W. A.; Okuda, J. *J. Mol. Catal.* **1987**, *41*, 109−122. (b) Herrmann, W. A.; Herdtweck, E.; Flöel, M.; Kulpe, J.; Küsthardt, U.; Okuda, J. *Polyhedron* **1987**, *6*, 1165−1182. (c) Gable, K. P.; Phan, T. N. *J. Am. Chem. Soc.* **1994**, *116*, 833−836. (d) Gable, K. P.; Juliette, J. J. J. *J. Am. Chem. Soc.* **1995**, *117*, 955−962.

(6) Liu, S.; Senocak, A.; Smeltz, J. L.; Yang, L.; Wegenhart, B.; Yi, J.; Kenttämaa, H. I.; Ison, E. A.; Abu-Omar, M. M. *Organometallics* **2013**, *32*, 3210−3219.

(7) Gable, K. P.; Ross, B. *ACS Symp. Ser.* **2006**, *921*, 143−155.

(8) Felixberger, J. K.; Kuchler, J. G.; Herdtweck, E.; Paciello, R. A.; Herrmann, W. A. *Angew. Chem., Int. Ed. Engl.* **1988**, *27*, 946−948.

(9) (a) Harms, R. G.; Herrmann, W. A.; Kühn, F. E. *Coord. Chem. Rev.* **2015**, *296*, 1−23. (b) Espenson, J. H.; Yiu, D. T. Y. *Inorg. Chem.* **2000**, *39*, 4113−4118. (c) Abu-Omar, M. M.; Espenson, J. H. *Inorg. Chem.* **1995**, *34*, 6239−6240. (d) Abu-Omar, M. M.; Appelman, E. H.; Espenson, J. H. *Inorg. Chem.* **1996**, *35*, 7751−7757. (e) Lahti, D. W.; Espenson, J. H. *Inorg. Chem.* **1999**, *38*, 5230−5234.

(10) (a) Herrmann, W. A.; Serrano, R.; Küsthardt, U.; Ziegler, M. L.; Guggolz, E.; Zahn, T. *Angew. Chem., Int. Ed. Engl.* **1984**, *23*, 515−517. (b) Gable, K. P.; Juliette, J. J. J.; Li, C.; Nolan, S. P. *Organometallics* **1996**, *15*, 5250−5251.

(11) Gable, K. P.; Juliette, J. J. J.; Gartman, M. A. *Organometallics* **1995**, *14*, 3138−3140.

(12) (a) Spek, A. L. *Acta Crystallogr., Sect. D: Biol. Crystallogr.* **2009**, *65*, 148−155. (b) The ring slippage Δ is calculated with the *PLATON* software as the distance between the ring centroid and the perpendicular projection of the metal on the least-squares plane of the ring.

(13) O'Connor, J. M.; Casey, C. P. *Chem. Rev.* **1987**, *87*, 307−318.

(14) Herrmann, W. A.; Küsthardt, U.; Flöel, M.; Kulpe, J.; Herdtweck, E.; Voss, E. *J. Organomet. Chem.* **1986**, *314*, 151−162.

(15) (a) Glendening, E. D.; Badenhoop, J. K.; Reed, A. E.; Carpenter, J. E.; Bohmann, J. A.; Morales, C. M.; Landis, C. R.; Weinhold, F. *NBO 6.0*; Theoretical Chemistry Institute, University of Wisconsin, Madison, WI, 2013; http://nbo6.chem.wisc.edu/. (b) All computational details, coordinates, and the full reference are given in the SI. Frisch, M. J. et al. *Gaussian 09*, revision D.01; 2013.

DOI: 10.1021/acs.inorgchem.5b02366
Inorg. Chem. 2015, 54, 11031−11036

(16) The analytical procedures and characterization of **2** are given in the SI, pp S5−S8.
(17) Laidler, K. J. *Chemical Kinetics*, 3rd ed.; Harper & Row: New York, 1987.
(18) (a) The glycol condensation experimental details and analytical data including the X-ray crystal structure for **4** are given in the SI, pp S13 and S14. (b) The bulky Cp^{ttt} ligand hinders the formation of rhenium(VII) diolate in contrast to what has recently been observed spectroscopically for MTO. Dethlefsen, J. R.; Fristrup, P. *ChemCatChem* **2015**, *7*, 1184−1195.

DOI: 10.1021/acs.inorgchem.5b02366
Inorg. Chem. 2015, 54, 11031−11036